The thickness and structure of dip coated polymer films in the liquid and solid states

Zhao Zhang, Fei Peng, Konstantin G Kornev*

Department of Materials Science and Engineering, Clemson University, Clemson, SC

29634

*kkornev@clemson.edu

Abstract

The films formed by dip coating of brass wires with dilute and semi-dilute solutions of Polyvinyl butyral in benzyl alcohol were studied in their liquid and solid states. While dilute and semi-dilute solutions behave as the Maxwell viscoelastic fluids, the thickness of liquid films follows the Landau-Levich-Derjaguin prediction for Newtonian fluids. At the very slow rate of coating, the film thickness was difficult to evaluate. Therefore, the dynamic contact angle was studied in detail. We discovered that polymer additives preserve advancing contact angle at its static value while receding contact angle follows the Cox-Voinov theory. In contrast, the thickness of solid films does not correlate with the Landau-Levich-Derjaguin predictions. Only solutions of the high molecular weight polymers form smooth solid films. Solutions of low molecular weight polymers may form either solid films with inhomogeneous roughness or solid polymer domains separated by the dry substrate. In technological applications, one could use very dilute polymer solutions of high molecular weight polymers to avoid inhomogeneities of solid films. These solutions form smooth solid films, and the film thickness can be controlled by experimental coating conditions.

Introduction

Advances in coating processes evolve in parallel with new technological advances and materials developments [1-4] and can be classified with respect to the processing protocols as dry processes (CVD, PVD, PECVD, etc.) [5, 6] and wet processes (spray coating, brush casting, spin coating, dip coating etc.) [7-10]. Among these coating methods, dip-coating is always attractive because of its simplicity, low-cost, and facile control[11, 12].

Dip coating of Newtonian viscous fluids on different substrates has been studied in various applications and significant progress in understanding of fluid mechanics of film formation has been achieved[11, 13-21]. Among different substrates, fibers and rods are the most challenging to coat: the curvature of the cylinder significantly influences the film deposition kinetics by altering the flow pattern in the meniscus region[22, 23]. One observes that the classical Landau-Levich-Derjaguin (LLD) theory of dip coating of fibers(see Eq.(10) below) can be used only in a narrow range of fiber radii, when the fiber radius R is much smaller than the capillary length $l = \sqrt{\frac{\sigma}{g\rho_l}}, \frac{R}{l} \le 0.13$, where ρ_l is the density of the liquid, g is the acceleration due to gravity, and σ is the surface tension[24]. This limitation adds to the difficulties of predicting the behavior of coating films formed from complex fluids such as polymer solutions.

In all wet coating processes including dip coating, one needs to control the final thickness of a coating layer after its solidification [12, 22, 25-32]. In many cases, the coating liquid is made of rheologically complex fluids [30, 31, 33-36] which are not easy to handle and evenly deposit on substrates. For example, almost all ceramic precursors for ceramic coatings, such as Al2O3, TiO2, and mullite precursors, either exhibit non-Newtonian features such as viscoelasticity [37] or nonlinear viscosity [38-40]. This complexity of the rheological behavior of coating liquids challenges materials scientists[12, 18, 23, 39, 41, 42]. Currently, films from polymer solutions demonstrating viscoelastic properties show the results that often contradict the existing theories [23, 43-45]. Even after achieving uniformity of liquid film, it remains a great challenge to convert this liquid film in a uniform and smooth solid layer [4, 12, 17, 30, 38, 46, 47]. At the same time, to satisfy the property requirements for electrical [48, 49], thermal [50], and optical [51] films on many devices, one needs to control the thickness and morphology of the remaining solid films. In general, there is no established relation between the thicknesses of the final solid film and the liquid film that has been originally deposited on the substrate[11].

To the best of our knowledge, there were no systematic studies of solid polymeric films in relation to their coating prehistory. Only recently, the deficiency in understanding of transition from liquid to solid films has been appreciated by materials scientists and new studies started to address this problem [4, 12, 17, 30, 38, 46, 47].

This paper aims to systematically analyze the effect of polymer additives on the properties of solid films formed by these polymers. We question how the engineering conditions of dip coating such as the speed of withdrawal of the rods and plates, viscosity and surface tension of the coating liquids will influence the thickness and morphology of solid films. To answer these questions, we 1) first study the effect of viscoelasticity on the thickness of the liquid film obtained by dip coating of rods and plates; 2) then we experimentally investigate the relation between the thickness of liquid and solid films questioning whether the LLD theory could correctly predict the thickness of the solid polymer film assuming that the evaporating solvent contributes to the film shrinkage proportionally to its volume fraction; 3) then we study the effect of molecular weight of the polymer on the morphology of the dried film.

To clearly see the effect of polymer additives on solution rheology, we use benzyl alcohol (Sigma-Aldrich, 99.8%), a Newtonian solvent that has: 1) sufficiently small viscosity (of the order of the water viscosity), so that the effect of polymer additives could be easily established; 2) negligible evaporation so that the mass gain after the dip coating of an article could be easily measured. The high molecular weight Polyvinyl butyral (PVB, Butvar B-72, Mw=175,000~250,000 Da) and low molecular weight PVB (Butvar B-98, Mw=40,000 and 70,000 Da), both are soluble at room temperature in benzyl alcohol were chosen as polymer additives. These polymers allowed us to study effects of polymer elasticity.

Experimental methods

Solution preparation

B72 (PVB, Butvar B-72, Mw=175,000~250,000 Da) and B98 (PVB, Butvar B-98, Mw=40,000~70,000 Da) were dissolved in benzyl alcohol and mixed by a magnetic stirrer. A series of solutions with the polymer concentration varying between 0 g/dL and 6g/dL for both B72 and B98 solutions were prepared. Solutions with low concentrations of polymers (0 g/dL, 0.25 g/dL, 0.5 g/dL, 1 g/dL) were used to

investigate the influence of solution viscoelasticity on the thickness of coating films in the liquid and solid states. Solutions with higher concentrations of PVB (1~6 g/dL) were also used to investigate the critical overlap concentration of the given polymer solution and the effect of polymer concentration on the solution viscoelasticity and, finally, on the film thickness.

Rheological properties

The surface tension of Newtonian liquids and polymer solutions with different concentrations of PVB in benzyl alcohol was measured using the pendant drop method by the KRUSS DSA10 instrument with a 0.5 mm needle at room temperature. The images of pendant drops were captured and analyzed using KRUSS DSA software.

The density of the fluids was calculated by measuring the weight of fluid in a fixed volume liquid pycnometer (25 ml) using an analytical balance (PI-214, Denver Instrument) at room temperature.

The viscosity of the Newtonian liquids was measured by a viscometer (Brookfield DV3THBCJ0). The viscosity of the polymer solution was measured using the capillary method. UBBELOHDE type viscometers were kept in a water bath (Cannon CT-1000) at 25°C, and a stopwatch was used to measure the efflux time. Here, the efflux time was maintained above 100 s in order to minimize the experimental error.

The critical overlap concentration c^* of the PVB-benzyl alcohol system was determined by the single point and multipoint methods.

To calculate the overlap concentration c^* by the single point method, the viscosity of the pure benzyl alcohol and the 1 g/dL PVB-B72 solution was measured. The intrinsic viscosity of PVB-B72 and overlap concentration in benzyl alcohol were determined as [52]:

$$[\eta] = \frac{\sqrt{2(\eta_{rel} - 1) - 2\ln \eta_{rel}}}{c}, \quad c^* = \frac{1}{[\eta]}$$
 (1)

where $\eta_{rel} = \frac{\eta}{\eta_0}$ is the relative viscosity; η is the viscosity of the polymer solution; c is the polymer concentration; η_0 is the viscosity of the pure solvent.

To determine the overlap concentration by the multipoint method, the viscosity vs. PVB concentration was plotted on a log-log scale. Then, the two power law fits were calculated for the data points on either side of the apparent slope change; at least 3 data points near this region were used for each fit. To determine the intersection of these fits, they were set equal, and the multipoint overlap concentration was calculated as the intersection point.

The viscoelasticity of a fluid can be characterized by its mean relaxation time. Figure 1a shows a schematic diagram of a filament break-up experiment using which, one can obtain the relaxation time by observing how the mid-diameter D_{mid} of a filament decreases with time[53-56]. For Newtonian fluids with no elasticity, the filament will neck down and break up rapidly due to the Rayleigh–Tomotika instability and D_{mid} will decrease linearly with time [57, 58]. However, for fluids with elasticity, this process will take a longer time, and D_{mid} should be proportional to $\exp\left(-\frac{t}{3\lambda_1}\right)$ [53-56] [59], where λ_1 is the relaxation time.

Using a homemade filament stretching device, a small quantity of fluid was first placed between two plates and then stretched by two needles moving apart very quickly. After stretching, a filament is formed between the ends of two plates, with its diameter D_{mid} decreasing with time. This process is recorded by high-speed cameras (MotionPro X3 and MotionPro Y) with a frame rate of up to 5000 frames per second.

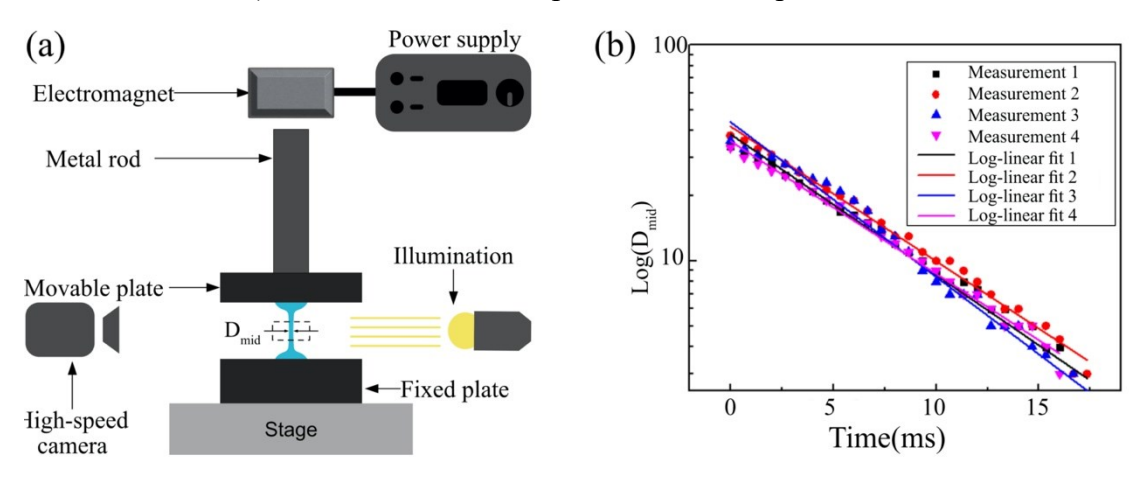


Figure. 1. (a) Schematic of the filament break-up experiment. (b) An example of the determination of relaxation time λ_1 based on the log-linear fit, $\log(D_{mid}) \propto (-t/(3\lambda_1))$ where

PVB B-72 in benzyl alcohol with a concentration of 4g/dL was used. Four measurements with the same solution on the same set-up were performed to find an average relaxation time.

Measurements of the thickness of liquid films

Brass wire with a radius of 0.255 mm, was chosen as the coating substrate. Before dip coating, all the wires were sonicated by an ultrasonicate cleaner (VWR Ultrasonic Cleaner 97043-964, 35 kHz, 90 W) in acetone for 2 hours and dried thoroughly.

The dip coater (KSV NIMA Dip Coater) was used to make these coatings. During the dip coating process, the wire was attached to the dip coater by a clamp. It was ensured that the wire was fixed vertically. The wire was lowered into the fluid reservoir at a velocity of 100mm/min. After reaching the targeted length, the wire was kept still for 15 seconds before withdrawal from the reservoir. Five withdrawal velocities (U = 20 mm/min, U = 50 mm/min, U = 100 mm/min, U = 200 mm/min, and U = 500 mm/min) were chosen to study the dependence of the coating thickness on the capillary number $Ca = U\eta/\sigma$.

The meniscus shape during the dip coating process was recorded using a high-resolution camera (Grasshopper 3, FILR, Wilsonville, OR); an example of the meniscus shape is shown in Figure 7a. It is shown that the meniscus videos have sufficient resolution to provide information on the shape of the meniscus close to the wire surface [60, 61].

The height and focus of the camera were adjusted so that the horizontal air-liquid interface could be captured, and the wire was sufficiently magnified. The light source intensity and angle were carefully adjusted to make sure the meniscus shape and brass wire could be easily differentiated from the surroundings.

Parameters of the images, such as hue and brightness/contract, were adjusted using Photoshop to ensure that the profile of the meniscus boundary was clear and easily identified. (Figure 7a). These images were subsequently converted to black and white (Figure 7b) and analyzed to fit by the theoretical meniscus profile [62]:

$$z\left(\left(\frac{R+h}{R}\right)\right) = -\operatorname{Rcos}\theta\left[\ln\left(\left(\frac{R+h}{R}\right) + \sqrt{\left(\frac{R+h}{R}\right)^{2} - (\cos\theta)^{2}}\right) + \ln\left(\frac{e^{E}\sqrt{\beta}}{4}\right)\right] + \operatorname{Rcos}\theta\left[K_{0}\left(\left(\frac{R+h}{R}\right)\sqrt{\beta}\right) + \ln\left(\frac{R+h}{R}\right) + \ln\left(\frac{e^{E}\sqrt{\beta}}{2}\right)\right]$$

$$(2)$$

In this equation, z((R+h)/R) is the height of the meniscus profile at a certain radius (R+h) measured from the wire axis, θ is the contact angle, E=0.577215 is the Euler constant, $\beta = \frac{(\rho_l - \rho_g)gR^2}{\sigma}$ is the Bond number, $K_0(\frac{R+h}{R})$ is the Bessel function of the second kind. A Matlab code was developed to find the dynamic contact angle by adjusting the horizon line. Each side of the meniscus was examined, and the dynamic contact angle was reported as an average of these two. In Figure 7b we illustrate this procedure: the contact angle for the left side of the meniscus was found to be $\theta = 15^{\circ}$, while on the right side, it was $\theta = 18^{\circ}$. We thus report $\theta = (15^{\circ} + 18^{\circ})/2 = 16.5^{\circ}$. The error bar represents standard deviation of the contact angles measured in 3 repeats.

Measurements of thickness of dried films and their morphology

To study the morphology of dry films, we used an atomic force microscope (AFM, Alpha300, Witec Instruments Corp.). Since the curvature of brass wire is high, it is difficult to scan its surface with AFM. Therefore, we prepared flat substrates for this

purpose. Silicon wafers (WRS Materials) were used as substrates. The Si wafers were first cut into 10 mm*50 mm pieces by a diamond cutter. They were cleaned in an ultrasonic bath (VWR Symphony) for 30 min with deionized water. Subsequently, the wafers were placed in a hot (~60 °C) "piranha" solution (3:1 concentrated sulfuric acid/30% hydrogen peroxide) for 1h sonication. Then, the wafers were rinsed several times with high purity deionized water and stored in deionized water. Before the use, the substrates were dried under a stream of dry high purity nitrogen (National Specialty Gases).

To confirm that the Si wafers have the same wetting properties as those of our wires, with Krüss, FM40MK2 Easydrop we measured the contact angles that the sessile drops of PVB solutions formed with them. The solutions of the lowest and highest concentrations (0.25 g/dL PVB-B72 and 1 g/dL PVB-B72) were used for comparison of their contact angles. These solutions have very similar surface tensions (Table 1&2). The advancing contact angles of 0.25g/dL PVB-B72 and 1g/dL PVB-B72 on Si wafers were 21.0° ± 0.32° and 21.1° ± 0.49° respectively, which are very similar to the advancing contact angle of PVB solution on brass wire (~22°). Thus, the solutions with intermediate concentrations of polymers are expected to show similar contact angles. These results confirmed that the adhesion characteristics of Si wafers should be similar to those of brass wires and hence the AFM results should provide useful insight into the morphology of films obtained on brass wires.

The dip coater (KSV NIMA Dip Coater) was used to reproduce coatings on the Si wafer. During the dip coating process, the Si wafer was attached to the dip coater by a clamp. It was ensured that the wafer was fixed vertically. The coating procedure explained in the previous section was strictly followed.

The coated substrates were dried vertically in the oven at 80°C overnight.

To measure the coating thickness after drying, we scratched the solid film along the vertical line in the center of the substrate. The edges of the scratched trenches were scanned using an atomic force microscope (AFM, Alpha300, Witec Instruments Corp.) to obtain the difference in height between the center of the surface of the PVB coating and the substrate. The thickness of the coating was measured at the position of 15mm

from the bottom of the substrate. The thickness profile along the vertical dimension was obtained by measuring the thickness from position 2.5 mm to position 27.5 mm with a step of 2.5 mm.

The coating thickness and roughness of the coating was evaluated by Gwyddion open source software. To calculate the roughness, 5 lines were drawn on the AFM image. The root mean square roughness (R_q) was then evaluated by the software following its definition:

$$R_{q} = \sqrt{\frac{1}{n} \sum_{i=1}^{n} y_{i}^{2}}$$
 (3)

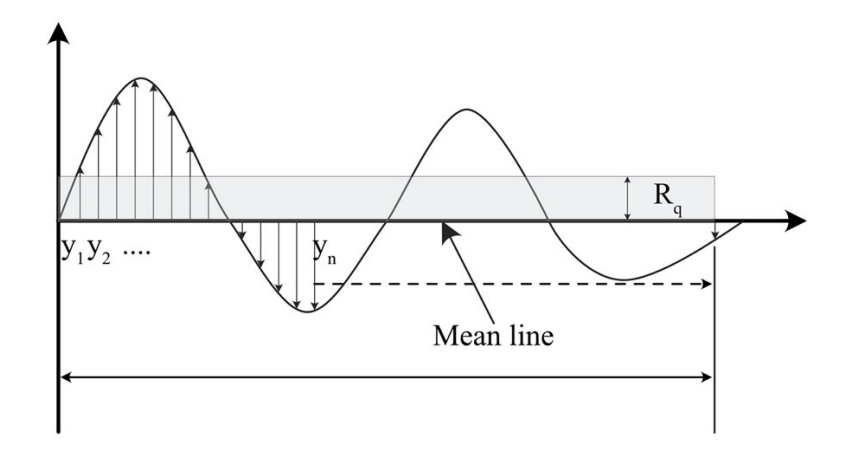


Figure 2. Geometrical meaning of the root mean square roughness R_q . The heights y_i , i = 1,2,3...n were measured at different positions along the coating film to evaluate R_q using Eq.(3)

Due to the film drainage [63] and the edge effects during the drying process, the coating thickness of the dried film follows a parabolic profile along the vertical coordinate. This profile follows the Jeffreys expression for post-withdrawal drainage of a Newtonian fluid [64]

$$h(z,t) = \left(\frac{\eta z}{\rho g t}\right)^{1/2} \tag{4}$$

If we neglect the end droplet and assume that the profile of a liquid film is parabolic, the average coating thickness at any time t is obtained as

$$\bar{h}(t) = \frac{1}{L} \int_0^L \left(\frac{\eta z}{\rho g t}\right)^{1/2} dz = \frac{2}{3} \left(\frac{\eta}{\rho g t}\right)^{1/2} L^{1/2}$$
 (5)

where L is the coating length. Solving Eq. (5) for t and plugging the result in Eq. (4), we obtain the position $z_{\bar{h}}$ as

$$z_{\overline{h}} = \frac{4}{9}L\tag{6}$$

This position specifies the place where to find an average coating thickness, (Figure 3). In our experiment, the coating length was L=35 mm, which gives $z_{\bar{h}}\approx 15.5$ mm. Thus, our selection of the measurement position (15mm) can reflect the "dry" coating thickness of the sample:

$$\bar{h}_{dry} \approx h(15mm)_{dry} \tag{7}$$

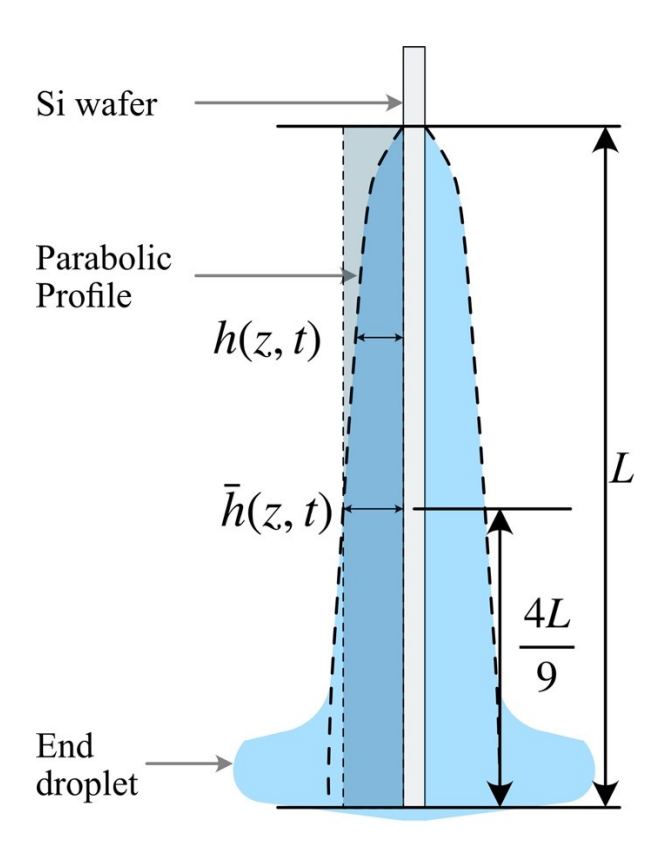


Figure 3. Diagram of the parabolic profile of the coating thickness after film draining at time t.

The theoretical "dry" coating $h_{\infty dry}$ thickness is calculated as

$$h_{\infty dry} = \frac{V_P h_{\infty p}}{V_P + V_S} = \frac{\frac{m_P}{\rho_P} h_{\infty p}}{\frac{m_P}{\rho_P} + V_S} = \frac{c_P h_{\infty p}}{c_P + \rho_P}$$
(8)

where c_P is the polymer concentration in solvent $(c_P = \frac{m_P}{V_S})$; ρ_P is the density of the polymer; $h_{\infty p}$ is the coating thickness based on LLD theory for plates, given as

$$h_{\infty p} = A_{plate} \cdot l \cdot Ca^{\frac{2}{3}}, \quad A_{plate} = 0.945, \quad Ca = U \eta/\sigma, \quad l = \sqrt{\frac{\sigma}{g\rho_l}} \quad (9)$$

Results and discussion

Density, surface tension, and viscosity

Table 1 and

Table 2 shows the surface tension, density, and calculated capillary length of PVB solutions with various concentrations. And Table 3 and Table 4 report the solution viscosity.

Table 1. Density of B72-benzyl alcohol solutions

B72 Concentration (g/dL)	0	0.25	0.5	1
Density (g/cm ³)	1.04	1.04	1.04	1.04
Surface tension (mN/m)	37.5	37.3	37.7	37.6
Capillary length (mm)	1.918	1.913	1.923	1.920

Table 2. Density of B98-benzyl alcohol solutions

B98 Concentration (g/dL)	0	0.25	0.5	1
Density (g/cm ³)	1.04	1.04	1.04	1.04
Surface tension (mN/m)	37.5	37.5	37.4	37.6
Capillary length (mm)	1.918	1.918	1.915	1.920

Table 3. Viscosity of B72-benzyl alcohol solutions

[B-72] (g/dL)	0	0.1	0.2	0.3	0.4	0.5	0.6	0.7	0.8	1
Viscosity (cP)	5.74	6.40	7.82	8.9	10.1	11.2	13.2	14.7	17.2	21.0

Table 4. Viscosity of B98-benzyl alcohol solutions

[B-98] (g/dL)	0	0.25	0.5	1	1.2	1.5	1.75	2	2.5	3
Viscosity (cP)	5.74	6.9	7.2	10.8	13.7	15.1	16.5	18.5	28.8	32.8

Based on these data, we conclude that the addition of small quantities of PVB to benzyl alcohol doesn't cause much change of the surface tension, density and the capillary length of the solution. Plotting viscosity as a function of concentration in Figure 4a, one observes that the slope of the viscosity vs. PVB-B72 concentration changes suddenly between 0.5 g/dL and 0.6 g/dL, where the critical overlap concentration is located. After extending the regression lines below and above the critical overlap concentration, the precise value of c^* is determined to be 0.52 g/dL. The same method was applied to determine the critical overlap concentration of PVB-B98 (1.83 g/dL), Figure 4b.

Through the single point method [52], we found that the intrinsic viscosity of PVB-B72-benzyl alcohol system is 1.806 dL/g. Based on the relationship between the critical overlap concentration c^* and intrinsic viscosity $[\eta]$, we calculated that $[\eta]$ =0.56 g/dL

for B72, which is consistent with the multipoint method.

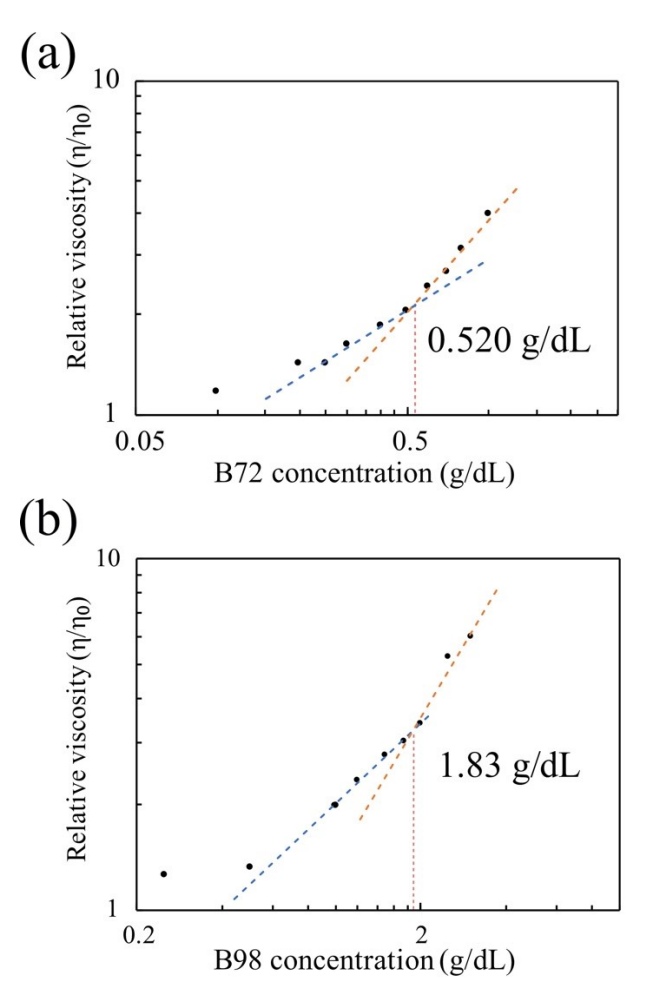


Figure 4. (a) Relative viscosity vs. PVB concentration in benzyl alcohol for high molecular weight PVB-B72. (b) Relative viscosity vs. PVB concentration in benzyl alcohol for low molecular weight PVB-B98

Relaxation time

The filament breakup process was monitored using a high-speed camera (Motion Pro X3, Princeton Instruments, NJ). An example (PVB-B72, 2 g/dL) of how the filament mid-diameter changes with time is shown in Figure 5a. These images were then analyzed with our Matlab code to determine the filament mid-diameter. The relaxation time λ_1 was determined by fitting D_{mid} with $\exp\left(-\frac{t}{3\lambda_1}\right)$ [59]. Figure 5 shows the linear change of the relaxation time with concentration of PVB. Considering that the measured $c^* = 0.52$ g/dL (PVB-B72) and $c^* = 1.83$ g/dL (PVB-B98), it is clearly seen that the Maxwell model with a single relaxation time can describe the solutions far above the critical overlap concentration.

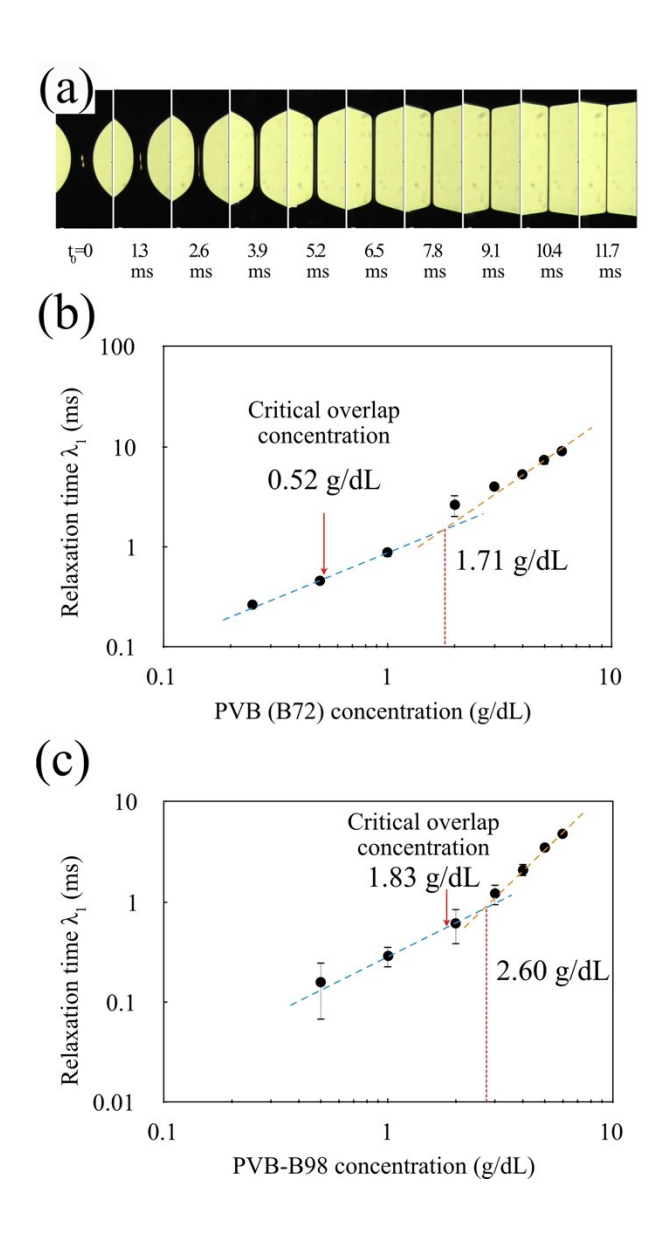


Figure 5. (a) Filament break-up experiment with PVB-B72 (2 g/dL) in a benzyl alcohol solution. (b) Concentration dependence of relaxation time for high molecular weight PVB-B72. (c) Concentration dependence of relaxation time for low molecular weight PVB-B98

Effect of solution viscoelasticity on the coating thickness

Our results in Figure 6 show that the film thickness $h_{\infty f}$ extracted from the measurements of flux q as discussed in detail in our recent publication [24], follows the LLD theory for fibers $(h_{\infty f})$ when $Ca > 10^{-4}$:

$$h_{\infty f} = A_{fiber} \cdot R \cdot Ca^{\frac{2}{3}}, \ A_{fiber} = 1.34. \tag{10}$$

No discrepancy with the Newtonian behavior was found when we plotted the film thickness versus capillary number, Figure 6. Neither high molecular weight PVB-B72 nor low molecular weight PVB-B98 show any significant deviation from the LLD theory. The data obtained on lower capillary numbers ($Ca < 10^{-4}$) must be taken with a precaution as the films were very thin and hence an incremental change of the weight of brass wires was difficult to measure accurately because of the limitation of our semi-micro balance.

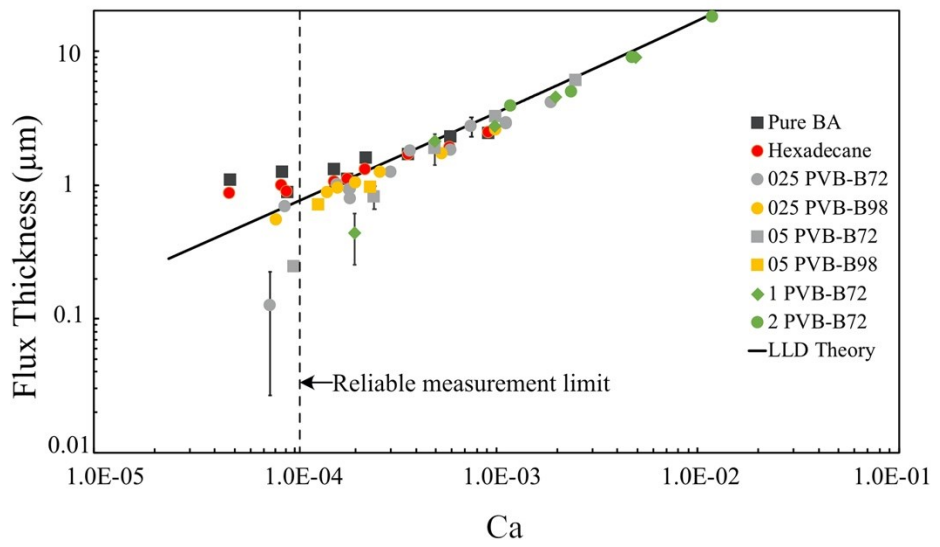


Figure 6. The film thickness $h_{\infty f}$ on a brass wire (R=0.255mm) vs capillary number. Pure viscous fluids (Pure BA, Hexadecane) and viscoelastic fluids (PVB-BA solutions) were examined. The solid line is Eq. (10), the LLD theory for fibers $(h_{\infty f})$. The data on the right side from the dashed vertical line have the greatest accuracy with the given methodology.

To explain the observed trend, we compared the characteristic time associated with the shearing of liquid in the film and the time associated with the extension of polymers in the shear flow. The shear rate in the dip-coating process can provide a reasonable estimate of the characteristic time for the polymer extension:

$$t_{viscous} = \frac{h}{U}. (11)$$

Taking $h = h_{\infty f} \sim 20 \mu m$ and at the maximum withdrawal velocity $U = 500 \ mm/min$, we have $t_{viscous} \approx 2.4 \times 10^{-3} \text{s}$. The relaxation time of our polymer solutions is less than one millisecond, $\lambda_1 < 10^{-3} \ \text{s}$. Therefore, the ratio $\frac{\lambda_1}{t_{viscous}}$ "1. This small ratio indicates that during the coating process, the polymer has time to relax. Hence, any

elastic effects of polymer coils can be safely ignored in this range of speeds of dip coating.

Dynamic contact angle

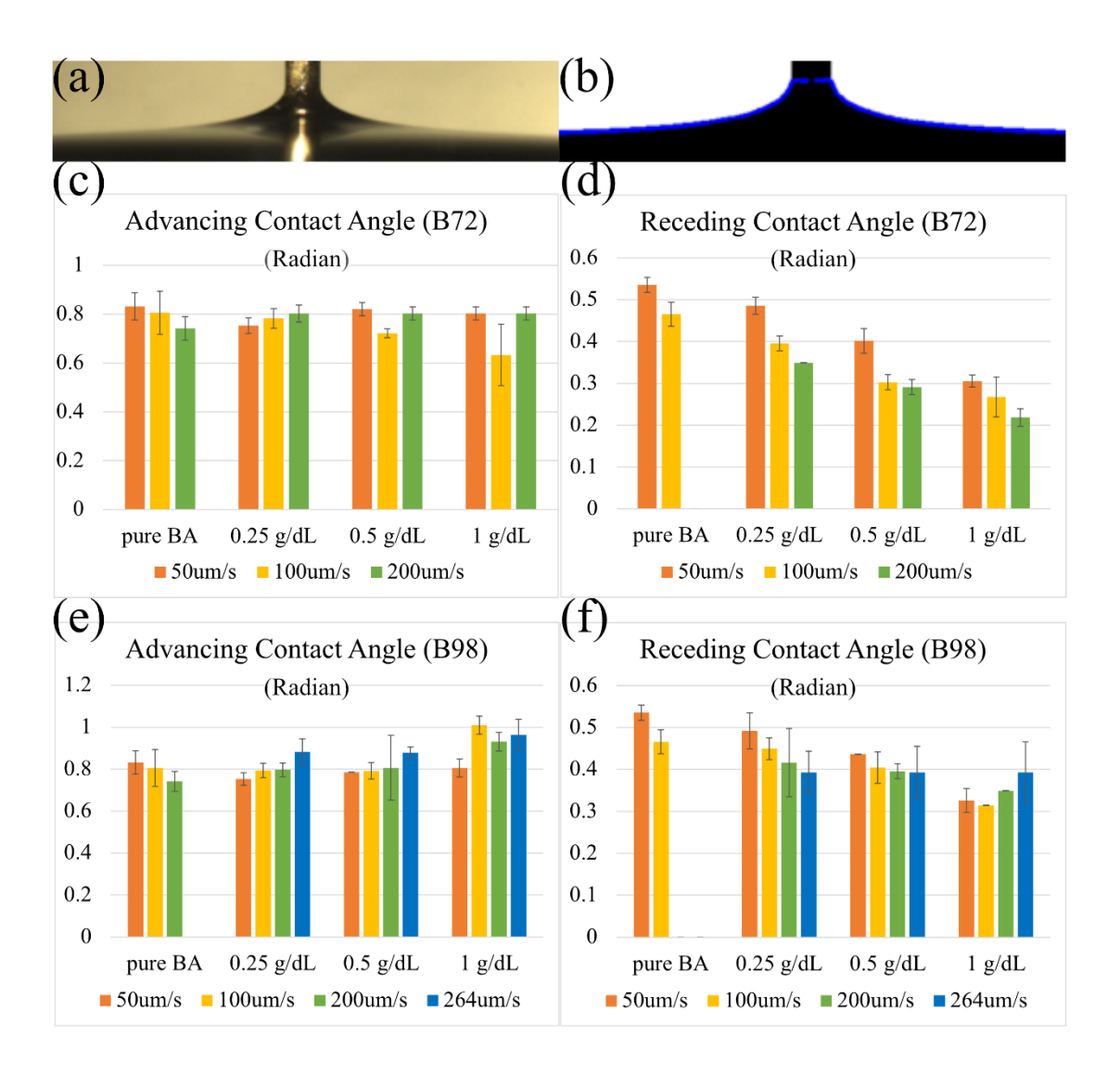


Figure 7. (a) An example of an image of a receding meniscus (1 g/dL Polyvinyl butyral, 100 μm/s); (b) The best fit of meniscus profile by Eq. (2) (left part: 15°, right part 18°). (d) The resulting advancing and receding dynamic contact angles of PVB solutions at different concentrations, velocities, and molecular weights of PVB.

Figures 7(c)-(f) show the effect of polymer concentrations and velocities on advancing and receding dynamic contact angles for both the high molecular weight

PVB and the low molecular weight PVB. For advancing dynamic contact angle, there is no clearly observable differences between molecular weights. For receding contact angle, the higher the molecular weight polymer, the stronger its velocity dependence. Thus, at the same polymer concentration, the greater the solution viscosity the smaller the receding contact angle.

As shown in Figure 7, the continuum fluid mechanics theory does explain the relations between the coating thickness and capillary number. We therefore apply the same type continuum fluid mechanics model, the Cox-Voinov model [65] of dynamic contact angle, to understand the obtained trends in Figure 7. In the fluid mechanics theory, the apparent dynamic contact angle θ_{dyn} is predicted by the Cox-Voinov model as

$$\theta_{dyn}^3 = \theta_0^3 \pm ACa,\tag{12}$$

where A is a positive constant and θ_0 is the static advancing contact angle when the substrate is not moving. The positive sign in Eq. (12) refers to the advancing meniscus and the negative sign refers to the receding meniscus. The angle θ_0 is obtained by setting the velocity of the moving contact line to be zero U = 0, i.e. Ca=0. Equation (12) suggests that the cubed dynamic angle should depend linearly on the velocity of the moving wire and the slope of this dependence should not depend on the direction of wire movement. In Figure 8 we plot the experimental dynamic contact angles versus log Ca to cover the entire range of capillary numbers [66, 67].

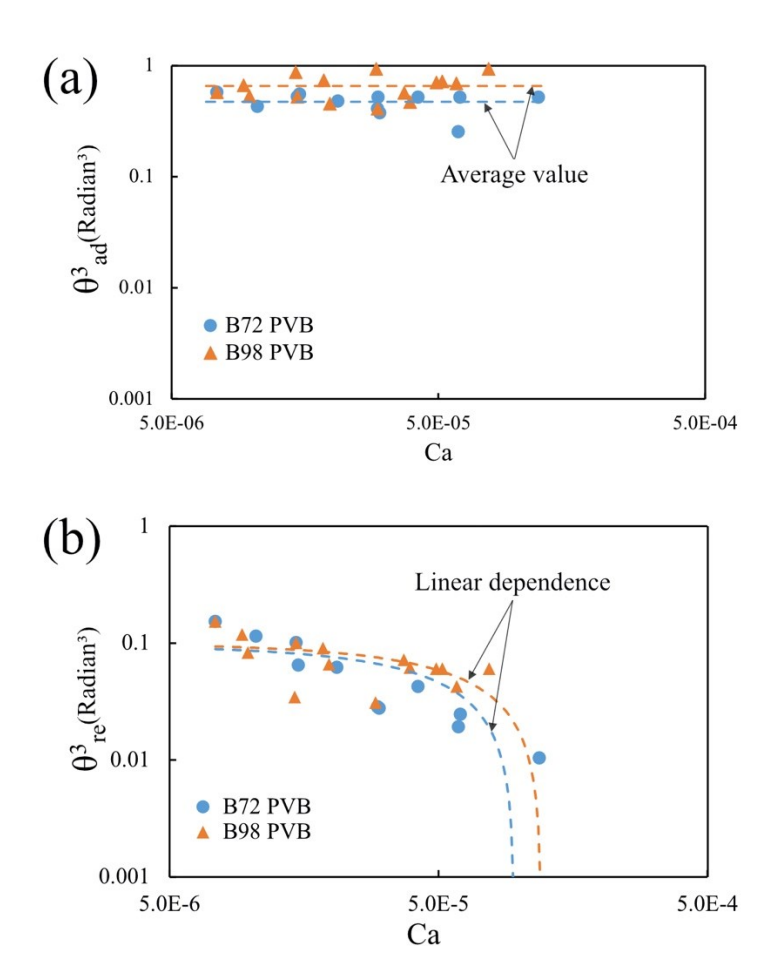


Figure. 8. The capillary number dependence in the logarithmic scale of (a) advancing dynamic contact angle θ_a and (b) receding dynamic contact angle θ_r . To guide the reader, the dashed curves corresponding to the linear dependences are shown as well.

In contrast to the Cox-Voinov prediction, in the range of capillary numbers, 10^{-6} < Ca< 10^{-4} where the theory should work, the advancing contact angle (Figure. 8a), does not depend on capillary number. The receding contact angle (Figure. 8b) does depend on capillary number and it does decrease linearly as the capillary number increases. Thus, within the studied range of capillary numbers, one would not see any elastic contribution of polymers when the wire is withdrawn from polymer solutions. We did not observe any behavior similar to those reported in the literature [68] that have been associated with the solvent evaporation and polymer concentration at the receding contact line. In contrast, dipping the wire into solution, one would observe some deviation from the Newtonian behavior suggesting that polymer interacts stronger within the liquid wedge in this mode of movement and the fluid flow is screened by the polymer chains preserving equilibrium shape of meniscus.

Coating thickness of solid vs. liquid films

Figure 9a is an example of the edge profile of scratch trench taken by AFM and analyzed by Gwyddion. The thickness of the solid film was measured by calculating the height difference at the edge of the step. The thickness along the vertical dimension followed a parabolic profile (Figure 9b). The only exceptions are given by the measurements taken at the points that are very close to the bottom edge (Position = 2.5 mm). At this position, the drained fluid carrying the polymer was gathered into a big drop before the solvent has completely evaporated.

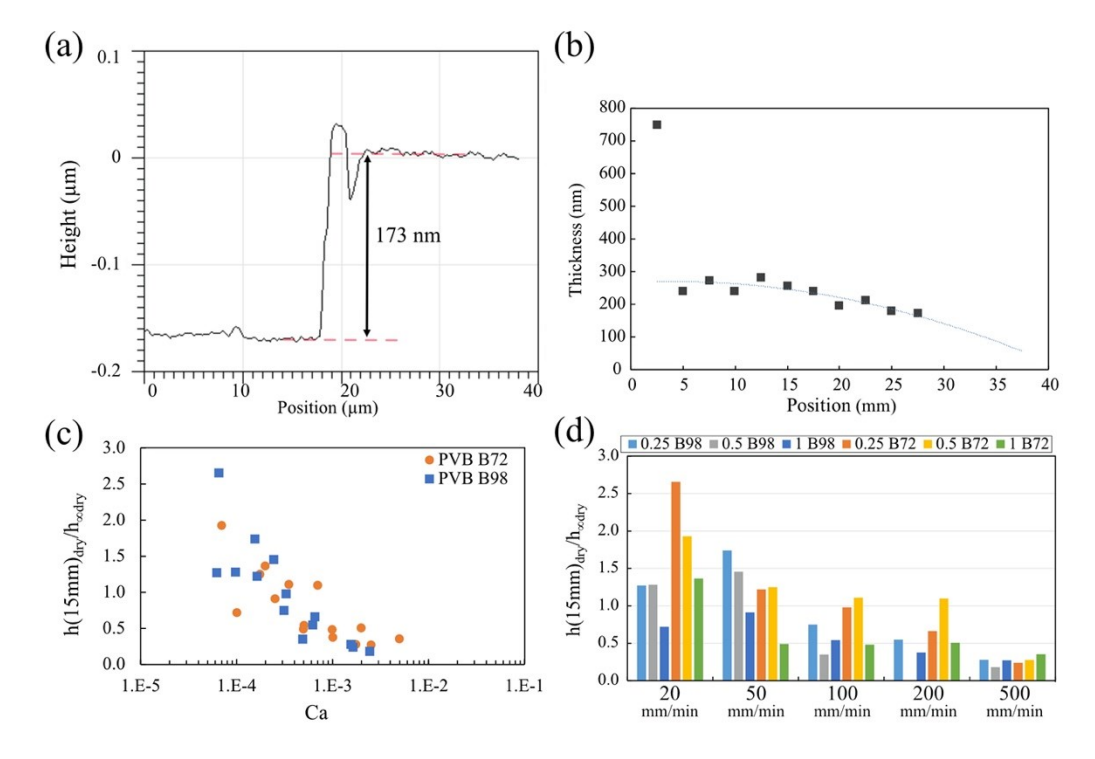


Figure 9. (a) The AFM edge profile of the scratched trench. The coating was prepared with 1 g/dL PVB-B72 at a withdrawal velocity of 500 mm/min. (b) The profile of solid film along the vertical direction of the coated plate. (Position=0 is at the bottom; position=35 mm is at the top edge of the coating film). (c) The ratio of measured thickness of the solid film at position 15mm ($h(15mm)_{dry}$) and the thickness based on LLD theory $h_{\infty dry}$ (defined in Eq. (8) and Eq. (9) vs. Capillary number. (d) The ratio of measured thickness of the solid film at position 15 mm ($h(15mm)_{dry}$) over the "dry" coating thickness based on LLD theory $h_{\infty dry}$ (defined in Eq. (8) and Eq. (9)) for different polymer concentrations and withdrawal velocities

As shown in Figure 9 b), the film thickness at the heights between 10 mm and 18 mm does not change significantly. Therefore, we analyze the dependence of the

thickness of the dry film at height 15 mm, h (15mm) $_{dry}$. With increasing capillary number, the ratio $\frac{h \ (15mm)_{dry}}{h_{\infty dry}}$ decreases (Figure 9c and Figure 9d) suggesting that the theory overestimates the thickness of the dry film. Since the surface tensions of low and high molecular weight polymers are the same, the main contribution to the capillary number comes from viscosity and speed of the plate withdrawal. In Figure 9d) we attempted to separate these two contributions replotting the data as a bar chart. We observe that the theoretical prediction $\frac{h \ (15mm)_{dry}}{h_{\infty dry}} \sim 1$ for low molecular weight solutions works only for very low speed of plate withdrawal, 20 mm/min and for low polymer concentration $< 1 \ g/dL$. At greater withdrawal speed, the high molecular weight solutions perform better. But the effect of polymer concentration becomes important: in the range of withdrawal speed from 50 mm/min to 200 mm/min, only polymer solutions with the concentration near the critical overlap concentration ($\sim 0.5 \ g/dL$) follow theoretical prediction. As the withdrawal speed decreases, the dilute solutions make the film thickness thicker than expected.

These data have to be interpreted with some caution. Indeed, as shown by Eq. (4), the coating thickness at position z will decrease with time due to the film drainage. At greater capillary number, i.e. at greater withdrawal speed or smaller viscosity, the thickness of the coating film formed during the dip-coating process should be thicker. Therefore, it took a longer time for the thicker film to dry and more polymer gathered at the bottom edge of the plate. The drainage effect on the coating thickness is especially significant because the solvent in our system (benzyl alcohol) has a very low evaporation rate.

Coating thickness vs. coating roughness

For high molecular weight PVB-B72, the thickness of dried films varied from 13nm to 173nm. For all these samples, the roughness of the coating surface was very low $(R_q < 1 \text{ nm})$ (Figure 10a and Figure 11a).

However, for the low molecular weight PVB-B98 polymer, the roughness of the solid coating showed a thickness dependence (Figure 10b and Figure 11b). For coatings

thicker than 40nm, the surface roughness was low ($R_q < 1 \text{ nm}$). As the coating thickness decreased, the surface roughness rose quickly ($\sim 7 \text{ nm}$). The higher roughness is related to the formation of nodules and nodule aggregates shown by the AFM scans (Figure 11b). These nodules and nodule aggregates are formed most likely due to the convection cells caused by surface tension gradients [69]. Scriven *et al.* [70] found that for thinner films, the surface tension driven convection can be initiated by smaller temperature differences. On the other hand, the viscosity can resist convective flow [69] and stabilize the coating.

The critical overlap concentrations for PVB-B72 and PVB-B98 were $c^* = 0.52$ g/dL and $c^* = 1.83$ g/dL, respectively. Therefore, all polymer solutions used here (except for PVB-B72 1 g/dL) were classified as being dilute or semi-dilute polymer solutions. The viscosity of the solution was also small. During solvent evaporation, the concentration of the polymer in the film increases. In solutions of the high molecular weight polymer (PVB-B72), the viscosity increased rapidly with the concentration (Fig. 4a). Therefore, as evaporation proceeds, the rapidly increased viscosity resists the development of film instability. As a result, a smooth solid film remains deposited on the substrate (Figure 10a and Figure 11a).

In contrast, in solutions of the low molecular weight polymer (PVB-B98), the viscosity increased more slowly with concentration (Fig 4b). In very thin films, less than 40 nm thickness, this effect of low molecular weight polymers becomes critical in shaping the solid films. In these films, polymer coils do not have time to concentrate: evaporation of the solvent is fast and the dried islands prevent the formation of entanglements between polymers. Due to the slow increase of viscosity and the lack of polymer entanglements in dilute and semi-dilute polymer solutions, any perturbations of the air-liquid interface during film evaporation were not effectively damped. As a result, nodules and nodular aggregates have been formed in the thin films, Figure 10b and Figure 11b. The film's roughness increased.

When the coating thickness of solutions of the low molecular weight polymer (PVB-B98) increased above > 40nm, the resulted solid film was again smooth. This suggests

that over time, the solvent from dilute or semi-dilute polymer solutions evaporate gradually increasing the solution concentration and hence polymer entanglements. The rapid increase of viscosity and significant entanglements of polymers effectively resist the development of perturbations on the air-liquid interface leading to a smoother solid film.

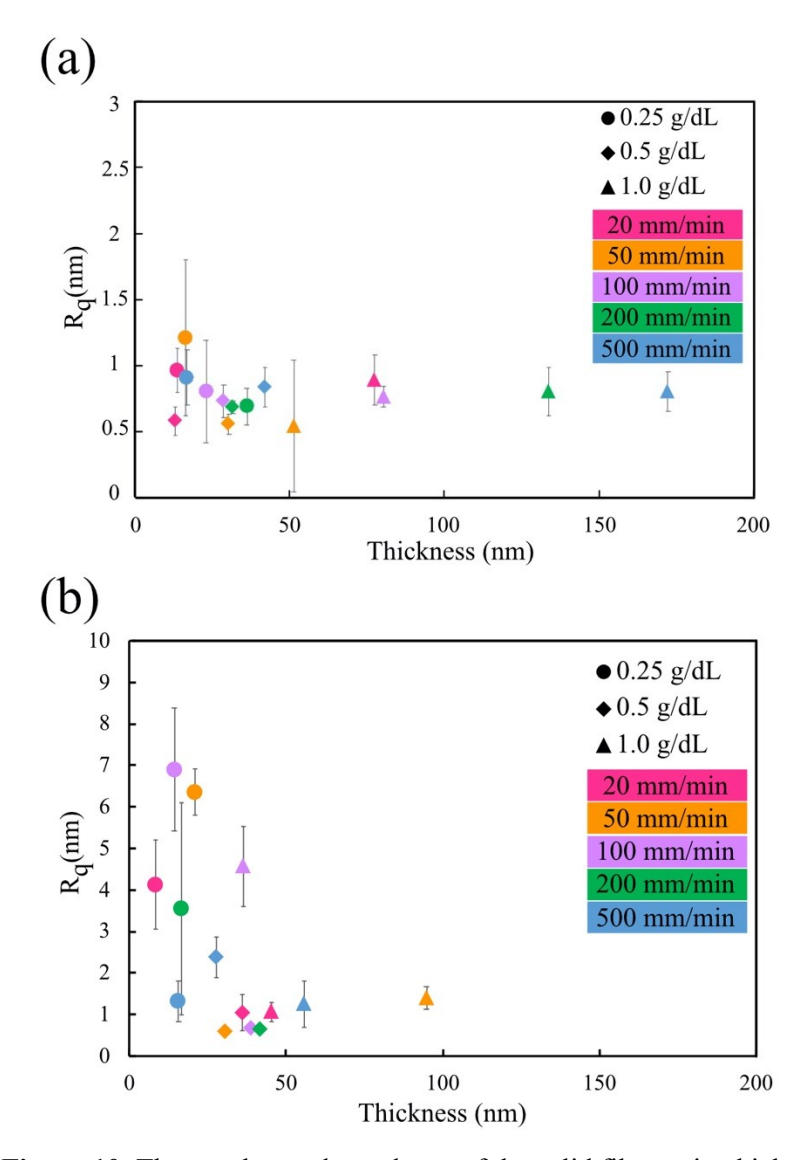


Figure 10. The roughness dependence of the solid film on its thickness (a) high molecular weight PVB(B72) solution. (b) low molecular weight PVB(B98) solution

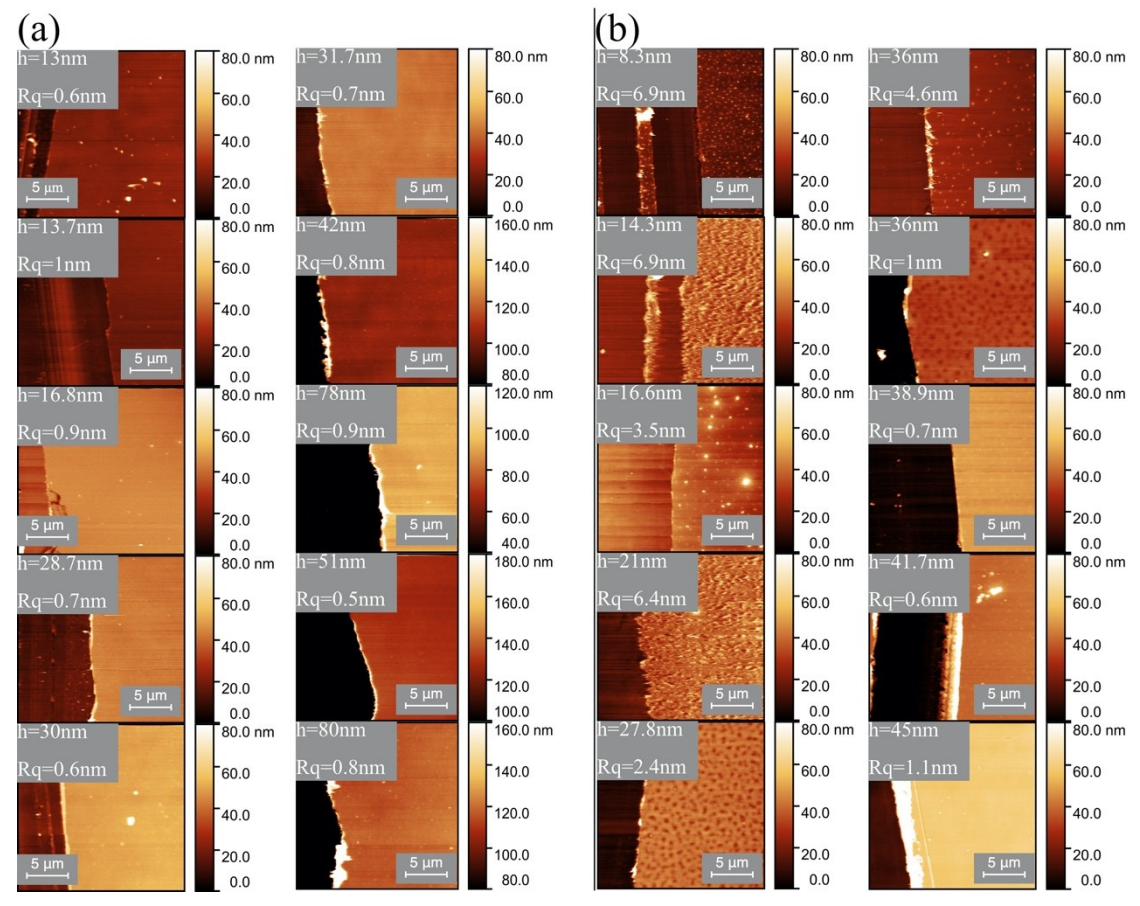


Figure 11. (a) AFM images showing the morphology of solid films obtained from the high molecular weight polymer (B72). The films with different thicknesses have smooth surfaces. (b) AFM images showing the morphology of solid films obtained from the low molecular weight polymer (B98). Thin films have bumpy surfaces or form nodules. In each panel, the bright right part is the film, and the dark left portion is the trench.

Conclusion

We studied the effects of polymer additives on the thickness of coated films in their liquid and solid states. The films were formed by dip coating of brass wires and Si wafers. As the coating liquids, we used solutions of Polyvinyl butyral in benzyl alcohol. To evaluate the effect of polymer elasticity and viscosity, solutions with different polymer concentrations were studied. Dilute and semidilute polymer solutions were investigated. The critical overlap concentration of high molecular weight polymer PVB-B72 and low molecular weight polymer PVB-B98 were determined to be 0.52 g/dL and 1.83 g/dL, respectively. The viscoelasticity of polymer solutions was evaluated using the liquid bridge breakup method. Both polymer solutions demonstrate the features typical for viscoelastic Maxwell fluid with a single relaxation time.

The coating thickness was studied for a broad range of capillary numbers, $10^{-6} < Ca = U\eta/\sigma < 10^{-2}$ specifying the effect of the speed U of withdrawal of the article, viscosity η of the coating film, and its surface tension, σ . It was found that the thickness of liquid films of the dilute and semi-dilute PVB polymer solutions was fully described by the Landau-Levich-Derjaguin theory. Thus, polymer viscoelasticity does not influence the thickness of the liquid films in the range of capillary numbers less than $Ca < 10^{-2}$.

Studying in detail the behavior of dynamic contact angles of the meniscus, we observed that in the range of capillary numbers $10^{-6} < \text{Ca} < 10^{-4}$, the advancing contact angle does not follow predictions of the Cox-Voinov theory formulated for Newtonian fluids. In this range of capillary numbers, the advancing contact angle remained constant, suggesting an important contribution of polymer elasticity preventing any flow from occurring in the liquid wedge adjacent to the contact line. The receding contact angle follows the Cox-Voinov predictions in accord with the success of the Landau-Levich-Derjaguin theory.

It was found that the coating films of slowly evaporating PVB solutions experience the effect of draining during the post-withdrawal evaporation. To study the film thickness in the region where the solid film has almost constant thickness, we applied the mixture rule for the thickness of liquid film and derived Eq.(8) relating the thickness of the dried film to the thickness of the liquid film. Using Eq.(8), we showed that the thickness of the dried film significantly deviates from the LLD theory prediction: Therefore, the estimates of the thickness of solid residual film based on the knowledge of the liquid film thickness cannot be justified.

To study the film surface morphology, we employed an Atomic Force Microscopy and prepared solid films on Si-wafers using the same dip coating method. The Si wafers had the same wetting properties as those of brass wires. For high molecular weight polymer coatings (PVB-B72), the dried films have smooth surfaces even at very low coating thickness (<10 nm). One can also form smooth solid films using solutions of the low molecular weight polymer (PVB-B98). But this smooth film can be obtained only when the coated films are thicker than 40 nm. In the very thin solid films (<40 nm)

obtained from the low molecular weight polymer (PVB-B98), one observes nodules and nodular aggregates, and the film surface is rough.

These results suggest that in a broad range of processing parameters, $10^{-6} < Ca = U\eta/\sigma < 10^{-2}$, the smooth solid films of the thickness less than hundreds of nanometers can be formed from dilute polymer solutions. The higher the polymer molecular weight, the thinner the film can be formed. The conditions for formation of uniform polymer films thinner than 40 nm remain unknown and further investigations are needed to reveal a possibility of forming nanometer thick films from low molecular weight polymers.

Acknowledgements

We thank Dr. Liying (Emma) Wei and Yueming Sun Z.Z. for helping with the characterization of Si wafers. and F.P would like to thank the funding support from NIH P20GM121342. K.G.K. was partially supported by National Science Foundation award IOS- 2042937 and the SC EPSCoR/IDeA Program under NSF Award No. OIA-1655740. The views, perspectives, and content do not necessarily represent the official views of the SC EPSCoR/IDeA Program nor those of the NSF.

REFERENCES

- [1] B. Fotovvati, N. Namdari, and A. Dehghanghadikolaei, "On Coating Techniques for Surface Protection: A Review," *Journal of Manufacturing and Materials Processing*, vol. 3, no. 1, 2019.
- [2] A. Kausar, "Polymer coating technology for high performance applications: Fundamentals and advances," *Journal of Macromolecular Science, Part A*, vol. 55, no. 5, pp. 440-448, 2018.
- [3] A. Zanurin, N. A. Johari, J. Alias, H. Mas Ayu, N. Redzuan, and S. Izman, "Research progress of sol-gel ceramic coating: A review," *Materials Today: Proceedings*, vol. 48, pp. 1849-1854, 2022.
- [4] G. Barroso, Q. Li, R. K. Bordia, and G. Motz, "Polymeric and ceramic silicon-based coatings a review," in *Journal of Materials Chemistry A* vol. 7, ed: Royal Society of Chemistry, 2019, pp. 1936-1963.
- [5] A. Mehta, H. Vasudev, and S. Singh, "Recent developments in the designing of deposition of thermal barrier coatings A review," *Materials Today: Proceedings*, vol. 26, pp. 1336-1342, 2020.

- [6] Z. Shen, G. Liu, R. Zhang, J. Dai, L. He, and R. Mu, "Thermal property and failure behavior of LaSmZrO thermal barrier coatings by EB-PVD," *iScience*, vol. 25, no. 4, p. 104106, Apr 15 2022.
- [7] D. Grosso, "How to exploit the full potential of the dip-coating process to better control film formation," (in English), *Journal of Materials Chemistry*, vol. 21, pp. 17033-17038, 2011.
- [8] P. Yimsiri and M. R. Mackley, "Spin and dip coating of light-emitting polymer solutions: Matching experiment with modelling," (in English), *Chemical Engineering Science*, vol. 61, pp. 3496-3505, 2006.
- [9] T. Justus *et al.*, "Oxidation Resistance and Microstructure Evaluation of a Polymer Derived Ceramic (PDC) Composite Coating Applied onto Sintered Steel," in *Materials* vol. 12, ed, 2019, p. 914.
- [10] M. V. Kelso, N. K. Mahenderkar, Q. Chen, J. Z. Tubbesing, and J. A. Switzer, "Spin coating epitaxial films," *Science*, vol. 364, no. 6436, pp. 166-169, Apr 12 2019.
- [11] S. E. Kistler and P. M. Schweizer, "Liquid film coating. Scientific principles and their technological implications." Glasgow, UK: Chapman & Hall, 1997, p.^pp. Pages.
- [12] D. Grosso, "How to exploit the full potential of the dip-coating process to better control film formation," *Journal of Materials Chemistry*, vol. 21, no. 43, pp. 17033-17038, 2011.
- [13] B. V. Derjaguin, "Thickness of the liquid film adhering to a moving thread," *Doklady Akademii Nauk Sssr*, vol. 39, p. 11, 1943.
- [14] L. D. Landau and V. G. Levich, "Dragging of a liquid by a moving plate," *Acta physicochimica URSS*, vol. 17, p. 42, 1942.
- [15] K. J. Ruschak, "COATING FLOWS," *Annual Review of Fluid Mechanics*, vol. 17, pp. 65-89, 1985.
- [16] S. J. Weinstein and K. J. Ruschak, "Coating flows," *Annual Review of Fluid Mechanics*, vol. 36, pp. 29-53, 2004.
- [17] J. J. Michels, K. Zhang, P. Wucher, P. M. Beaujuge, W. Pisula, and T. Marszalek, "Predictive modelling of structure formation in semiconductor films produced by meniscus-guided coating," *Nature Materials*, vol. 20, no. 1, pp. 68-75, Jan 2021.
- [18] S. Palma and H. Lhuissier, "Dip-coating with a particulate suspension," *Journal of Fluid Mechanics*, vol. 869, Jun 25 2019, Art. no. R3.
- [19] R. Sathyanath, A. Aarthi, and S. K. Kalpathy, "Liquid film entrainment during dip coating on a saturated porous substrate," *Chemical Engineering Science*, vol. 218, Jun 8 2020, Art. no. 115552.
- [20] L. Shaw *et al.*, "Manipulation and statistical analysis of the fluid flow of polymer semiconductor solutions during meniscus-guided coating," *Mrs Bulletin*, vol. 46, no. 5, pp. 380-393, May 2021.
- [21] H. M. J. M. Wedershoven, J. C. H. Zeegers, and A. A. Darhuber, "Polymer film deposition from a receding solution meniscus: The effect of laminar

- forced air convection," *Chemical Engineering Science*, vol. 181, pp. 92-100, May 18 2018.
- [22] D. Quere, "Fluid coating on a fiber," (in English), *Annual Review of Fluid Mechanics*, Review vol. 31, pp. 347-384, 1999.
- [23] E. Rio and F. Boulogne, "Withdrawing a solid from a bath: How much liquid is coated?," *Advances in Colloid and Interface Science*, vol. 247, pp. 100-114, Sep 2017.
- [24] Z. Zhang, A. Salamatin, F. Peng, and K. G. Kornev, "Dip coating of cylinders with Newtonian fluids," *J Colloid Interface Sci*, vol. 607, no. Pt 1, pp. 502-513, Sep 1 2021.
- [25] S. Obregón and V. Rodríguez-González, "Photocatalytic TiO2 thin films and coatings prepared by sol–gel processing: a brief review," *Journal of Sol-Gel Science and Technology*, vol. 102, no. 1, pp. 125-141, 2021.
- [26] S. Chen, Y. Deng, X. Xiao, S. Xu, P. N. Rudd, and J. Huang, "Preventing lead leakage with built-in resin layers for sustainable perovskite solar cells," *Nature Sustainability*, vol. 4, no. 7, pp. 636-643, 2021.
- [27] A. Jaafar, C. Hecker, P. Arki, and Y. Joseph, "Sol-Gel Derived Hydroxyapatite Coatings for Titanium Implants: A Review," *Bioengineering* (*Basel*), vol. 7, no. 4, Oct 14 2020.
- [28] A. Boukhari *et al.*, "Thickness effect on the properties of Mn-doped ZnO thin films synthesis by sol-gel and comparison to first-principles calculations," *Ceramics International*, vol. 47, no. 12, pp. 17276-17285, 2021.
- [29] M. Jiménez, A. Samie, R. Gadow, F. Kern, and J. Bill, "Siloxane Precursor-Based Protective Coatings for High Modulus Carbon Fibers in Ceramic Matrix Composites," *Ceramics*, vol. 1, no. 1, pp. 128-138, 2018.
- [30] F. A. Reifler, F. A. L. Sanchez, F. J. Clemens, K. Varga, and R. Hufenus, "Flexible ceramic-reinforced polyurethane composite coatings on synthetic fibres: Process of continuous liquid film coating and its influence on the coating thickness," *Composites Science and Technology*, vol. 70, no. 8, pp. 1207-1213, Aug 2010.
- [31] P. Yimsiri and M. R. Mackley, "Spin and dip coating of light-emitting polymer solutions: Matching experiment with modelling," (in English), *Chemical Engineering Science*, Article vol. 61, no. 11, pp. 3496-3505, Jun 2006.
- [32] K. G. Kornev and A. V. Neimark, "Hydrodynamic instability of liquid films on moving fibers," (in English), *Journal of Colloid and Interface Science*, Article vol. 215, no. 2, pp. 381-396, Jul 1999.
- [33] Y. Gu, Z. X. Chen, N. Borodinov, I. Luzinov, F. Peng, and K. G. Kornev, "Kinetics of Evaporation and Gel Formation in Thin Films of Ceramic Precursors," *Langmuir*, vol. 30, no. 48, pp. 14638-14647, Dec 2014.
- [34] A. Gans, E. Dressaire, B. Colnet, G. Saingier, M. Z. Bazant, and A. Sauret, "Dip-coating of suspensions," *Soft Matter*, vol. 15, no. 2, pp. 252-261, Jan 2019.

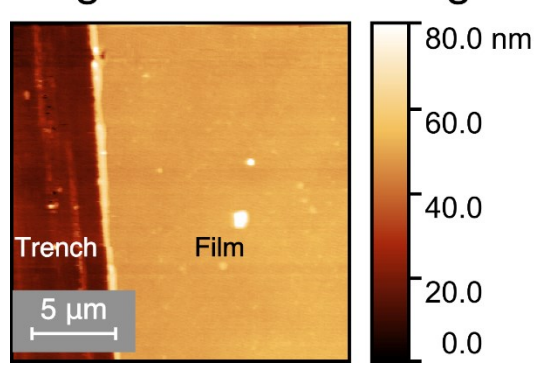
- [35] G. Berteloot, A. Daerr, F. Lequeux, and L. Limat, "Dip coating with colloids and evaporation," *Chemical Engineering and Processing-Process Intensification*, vol. 68, pp. 69-73, Jun 2013.
- [36] A. M. Karim, W. J. Suszynski, S. Pujari, L. F. Francis, and M. S. Carvalho, "Contact line dynamics in curtain coating of non-Newtonian liquids," *Physics of Fluids*, vol. 33, no. 10, Oct 2021, Art. no. 103103.
- [37] P. Colombo, G. Mera, R. Riedel, and G. D. Soraru, "Polymer-Derived Ceramics: 40 Years of Research and Innovation in Advanced Ceramics," (in English), *Journal of the American Ceramic Society*, Article vol. 93, no. 7, pp. 1805-1837, Jul 2010.
- [38] K. S. Wang, R. K. Bordia, and L. N. Brush, "A semi-empirical power-law model for the dip-coating of a substrate into a particle-containing, non-Newtonian, complex fluid system," (in English), *Ceramics International*, Article vol. 45, no. 6, pp. 6655-6664, Apr 2019.
- [39] M. Faustini, B. Louis, P. A. Albouy, M. Kuemmel, and D. Grosso, "Preparation of Sol-Gel Films by Dip-Coating in Extreme Conditions," *Journal of Physical Chemistry C*, vol. 114, no. 17, pp. 7637-7645, May 2010.
- [40] W. Y. Maeng, J. H. Yoon, and D. J. Kim, "Effect of process conditions (withdrawal rate and coating repetition) on morphological characteristics of sol-gel TiO2 film during dip coating," *Journal of Coatings Technology and Research*, vol. 17, no. 5, pp. 1171-1193, Sep 2020.
- [41] G. Berteloot, C. T. Pham, A. Daerr, F. Lequeux, and L. Limat, "Evaporation-induced flow near a contact line: Consequences on coating and contact angle," *Epl*, vol. 83, no. 1, 2008, Art. no. 14003.
- [42] D. D. Brewer, T. Shibuta, L. Francis, S. Kumar, and M. Tsapatsis, "Coating Process Regimes in Particulate Film Production by Forced-Convection-Assisted Drag-Out," *Langmuir*, vol. 27, no. 18, pp. 11660-11670, Sep 2011.
- [43] A. de Ryck and D. Quere, "Fluid coating from a polymer solution," (in English), *Langmuir*, Article vol. 14, no. 7, pp. 1911-1914, Mar 1998.
- [44] J. S. Ro and G. M. Homsy, "VISCOELASTIC FREE-SURFACE FLOWS THIN-FILM HYDRODYNAMICS OF HELE-SHAW AND DIP COATING FLOWS," (in English), *Journal of Non-Newtonian Fluid Mechanics*, Article vol. 57, no. 2-3, pp. 203-225, May 1995.
- [45] A. Abedijaberi, G. Bhatara, E. S. G. Shaqfeh, and B. Khomami, "A computational study of the influence of viscoelasticity on the interfacial dynamics of dip coating flow," (in English), *Journal of Non-Newtonian Fluid Mechanics*, Article vol. 166, no. 12-13, pp. 614-627, Jul 2011.
- [46] R. Balzarotti, C. Cristiani, and L. F. Francis, "Combined dip-coating/spin-coating depositions on ceramic honeycomb monoliths for structured catalysts preparation," *Catalysis Today*, vol. 334, pp. 90-95, Aug 2019.
- [47] R. K. Lade, K. S. Jochem, C. W. Macosko, and L. F. Francis, "Capillary Coatings: Flow and Drying Dynamics in Open Microchannels," *Langmuir*, vol. 34, no. 26, pp. 7624-7639, Jul 2018.

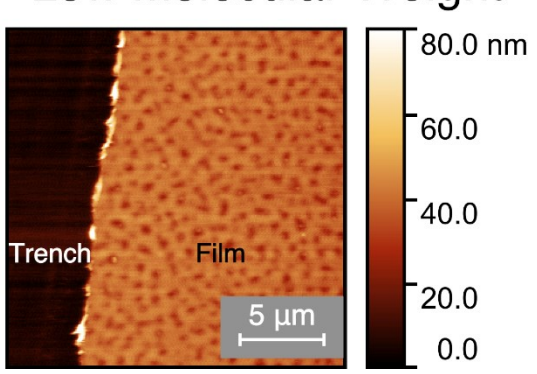
- [48] R. Baraka, "Thickness dependence of electrical and optical properties of sol gel ZnO coatings," in *Asian Journal of Chemistry* vol. 15, ed, 2003, pp. 1729-1734.
- [49] T. Nishioka *et al.*, "Influence of silver layer thickness on magnetization loss of YBCO coated conductors in transverse magnetic field with various orientations," in *Physica C-Superconductivity and Its Applications* vol. 412, ed, 2004, pp. 992-998.
- [50] H. Dai, X. H. Zhong, H. Y. Li, Y. F. Zhang, J. Meng, and X. Q. Cao, "Thermal stability of double-ceramic-layer thermal barrier coatings with various coating thickness," in *Materials Science and Engineering a-Structural Materials Properties Microstructure and Processing* vol. 433, ed, 2006, pp. 1-7.
- [51] L.-m. Huang, R.-j. Liu, C.-r. Zhang, Y.-f. Wang, and Y.-b. Cao, "Si/SiC optical coatings for C/SiC composites via gel-casting and gas silicon infiltration: Effects of carbon black content," in *Journal of Alloys and Compounds* vol. 711, ed, 2017, pp. 162-168.
- [52] O. F. Solomon and I. Z. Ciut, "Determination de la Viscosite Intrinseque de Solutions de Polymeres par une Simple Determination de la Viscosite," *Journal of Applied Polymer Science*, vol. 6, no. 24, pp. 683-686, 1962.
- [53] A. V. Bazilevskii, V. M. Entov, and A. N. Rozhkov, "Breakup of an Oldroyd liquid bridge as a method for testing the rheological properties of polymer solutions," *Polymer Science Series A*, vol. 43, no. 7, pp. 716-726, Jul 2001.
- [54] R. F. Liang and M. R. Mackley, "RHEOLOGICAL CHARACTERIZATION OF THE TIME AND STRAIN DEPENDENCE FOR POLYISOBUTYLENE SOLUTIONS," (in English), *Journal of Non-Newtonian Fluid Mechanics*, Article vol. 52, no. 3, pp. 387-405, Jun 1994.
- [55] J. M. Montanero and A. Ponce-Torres, "Review on the Dynamics of Isothermal Liquid Bridges," *Applied Mechanics Reviews*, vol. 72, no. 1, Jan 2020, Art. no. 010803.
- [56] L. E. Rodd, T. P. Scott, J. J. Cooper-White, and G. H. McKinley, "Capillary break-up rheometry of low-viscosity elastic fluids," *Applied Rheology*, vol. 15, no. 1, pp. 12-27, 2005.
- [57] M. P. Brenner, J. R. Lister, and H. A. Stone, "Pinching threads, singularities and the number 0.0304," (in English), *Physics of Fluids*, Article vol. 8, no. 11, pp. 2827-2836, Nov 1996.
- [58] J. Eggers, "Nonlinear dynamics and breakup of free-surface flows," (in English), *Reviews of Modern Physics*, Review vol. 69, no. 3, pp. 865-929, Jul 1997.
- [59] D. W. Bousfield, R. Keunings, G. Marrucci, and M. M. Denn, "NONLINEAR-ANALYSIS OF THE SURFACE-TENSION DRIVEN BREAKUP OF VISCOELASTIC FILAMENTS," (in English), *Journal of Non-Newtonian Fluid Mechanics*, Article vol. 21, no. 1, pp. 79-97, Apr 1986.

- [60] C. Huh and L. E. Scriven, "Shapes of axisymmetric fluid interfaces of unbounded extent," in *Journal of Colloid And Interface Science* vol. 30, ed, 1969, pp. 323-337.
- [61] Y. Wei, G. K. Seevaratnam, S. Garoff, E. Rame, and L. M. Walker, "Dynamic wetting of Boger fluids," in *J Colloid Interface Sci* vol. 313, ed, 2007, pp. 274-280.
- [62] M. M. Alimov and K. G. Kornev, "Meniscus on a shaped fibre: singularities and hodograph formulation," *Proceedings of the Royal Society a-Mathematical Physical and Engineering Sciences*, vol. 470, no. 2168, Aug 2014, Art. no. 20140113.
- [63] J. J. V. Rossum, "VISCOUS LIFTING AND DRAINAGE OF LIQUIDS," in *APPLIED SCIENCE RESEARCH* vol. 7, ed, 1958, pp. 121-144.
- [64] H. Jeffreys, "The Draining of a Vertical Plate," in *Mathematical Proceedings* of the Cambridge Philosophical Society vol. 26, ed, 1930.
- [65] O. V. Voinov, "Hydrodynamics of wetting," *Fluid Dynamics*, vol. 11, no. 5, pp. 714-721, 1977.
- [66] E. Rame and S. Garoff, "Microscopic and macroscopic dynamic interface shapes and the interpretation of dynamic contact angles," *Journal of Colloid and Interface Science*, vol. 177, no. 1, pp. 234-244, Jan 1996.
- [67] E. Rame, S. Garoff, and K. R. Willson, "Characterizing the microscopic physics near moving contact lines using dynamic contact angle data," *Physical Review E*, vol. 70, no. 3, Sep 2004, Art. no. 031608.
- [68] G. Jing, H. Bodiguel, F. Doumenc, E. Sultan, and B. Guerrier, "Drying of Colloidal Suspensions and Polymer Solutions near the Contact Line: Deposit Thickness at Low Capillary Number," *Langmuir*, vol. 26, no. 4, pp. 2288-2293, Feb 2010.
- [69] K. C. Khulbe, T. Matsuura, and S. H. Noh, "Effect of thickness of the PPO membranes on the surface morphology," *Journal of Membrane Science*, vol. 145, no. 2, pp. 243-251, 1998.
- [70] L. E. Scriven and C. V. Sternling, "On cellular convection driven by surfacetension gradients: effects of mean surface tension and surface viscosity," *Journal of Fluid Mechanics*, vol. 19, no. 3, pp. 321-340, 1930.

High Molecular Weight

Low Molecular Weight





For Table of Contents Only